^{18}F-PSMA Cerenkov Luminescence and Flexible Autoradiography Imaging in a Prostate Cancer Mouse Model and First Results of a Radical Prostatectomy Feasibility Study in Men

Pedro Fragoso Costa*[1,2], Lukas Püllen*[2,3], Claudia Kesch[2,3], Ulrich Krafft[2,3], Stephan Tschirdewahn[2,3], Alexandros Moraitis[1,2], Jan Philipp Radtke[2,3], Saskia Ting[4], Michael Nader[1,2], Jasmin Wosniack[1,2], David Kersting[1,2], Katharina Lückerath[1,2], Ken Herrmann[1,2], Wolfgang Peter Fendler[1,2], Boris Alexander Hadaschik[2,3], and Christopher Darr[2,3]

[1]Department of Nuclear Medicine, University Hospital Essen, Essen, Germany; [2]German Cancer Consortium–University Hospital Essen, Essen, Germany; [3]Department of Urology, University Hospital Essen, Essen, Germany; and [4]Institute of Pathology, University Duisburg–Essen, Essen, Germany

Intraoperative identification of positive resection margins (PRMs) in high-risk prostate cancer (PC) needs improvement. Cerenkov luminescence imaging (CLI) with ^{68}Ga-PSMA-11 is promising, although limited by low residual activity and artificial signals. Here, we aimed to assess the value of CLI and flexible autoradiography (FAR) with ^{18}F-PSMA-1007. **Methods:** Mice bearing subcutaneous PSMA-avid RM1-PGLS tumors were administered ^{18}F-PSMA-1007, and PET/CT was performed. After the animals had been killed, organs were excised and measured signals in CLI and FAR CLI were correlated with tracer activity concentrations (ACs) obtained from PET/CT. For clinical assessment, 7 high-risk PC patients underwent radical prostatectomy immediately after preoperative ^{18}F-PSMA PET/CT. Contrast-to-noise ratios (CNRs) were calculated for both imaging modalities in intact specimens and after incision above the index lesion. **Results:** In the heterotopic in vivo mouse model (n = 5), CLI did not detect any lesion. FAR CLI detected a distinct signal in all mice, with a lowest AC of 7.25 kBq/mL (CNR, 5.48). After incision above the index lesion of the prostate specimen, no increased signal was observed at the cancer area in CLI. In contrast, using FAR CLI, a signal was detectable in 6 of 7 patients. The AC in the missed index lesion was 1.85 kBq/mL, resulting in a detection limit of at least 2.06 kBq/mL. Histopathology demonstrated 2 PRMs, neither of which was predicted by CLI or FAR CLI. **Conclusion:** ^{18}F-PSMA FAR CLI was superior to CLI in tracer-related signal detectability. PC was could be visualized in radical prostatectomy down to 2.06 kBq/mL. However, the detection of PRMs was limited. Direct anatomic correlation of FAR CLI is challenging because of the scintillator overlay.

Key Words: flexible autoradiography; Cerenkov luminescence imaging; prostate cancer; margin assessment

J Nucl Med 2023; 64:598–604
DOI: 10.2967/jnumed.122.264670

Negative resection margins are a key component of tumor surgery in curatively intended interventions. Radical prostatectomy (RP) is one of the treatment options, along with radiotherapy, in men with localized or locally advanced prostate cancer (PC) (*1*). Positive resection margins (PRMs) occur in 11%–38% of patients undergoing RP, resulting in a higher risk of recurrence and disease-related mortality by a factor of 3 (*2,3*).

Preoperative MRI and nomograms have become widely used for local staging and for prediction of extracapsular extension. Recently, PSMA PET/CT was also included in the primary diagnosis of high-risk PC in the guidelines (*1*). Besides this, the use of intraoperative frozen section analysis reduces PRMs to 15% for all stages (*4–6*). Consequently, there is a wish to accurately detect malignant areas in real time during RP to ensure complete removal of PC.

For margin assessment, there currently are several newly implemented technologies with promising results, but some lack the large clinical studies required for subsequent use in clinical routine. Intraoperative conditions affecting the signal, long imaging times, and comparison with histopathology results are the main challenges (*7,8*).

Previously developed γ-counters are well established with single-photon–emitting radionuclides (*9*). Maurer et al. demonstrated reliable identification of small or atypically localized lesions for ^{99m}Tc-PSMA–guided surgery. The procedure has proven to be valuable for the successful intraoperative detection and removal of metastatic lesions in PC patients scheduled for salvage surgery (*10–13*).

The same technique has been successfully applied to β^+-emitters, giving way to potentially every radioligand in diagnostic PET/CT to be used in radioguided surgery (*14*). Other ex vivo imaging techniques, such as small-animal PET/CT for 3-dimensional analysis of lesions, which might provide volumetric information about the removed specimens, currently require further study-based investigation (*15*). In patients with biochemical recurrence, PSMA PET/CT demonstrates high accuracy, allowing surgical resection to be pursued for single lymph node metastases. Recently, the introduction of a so-called drop-in γ-probe has allowed for PSMA-guided surgery during minimally invasive robot-assisted surgery. Intraoperatively, γ-probes not only facilitate intraoperative in vivo guidance but also enable ex vivo measurements to confirm successful resection of

Received Jul. 14, 2022; revision accepted Oct. 27, 2022.
For correspondence or reprints, contact Christopher Darr (christopher.darr@uk-essen.de).
*Contributed equally to this work.
Published online Nov. 10, 2022.

these metastatic PC lesions, with a specificity of more than 95% for ^{99m}Tc-PSMA-I&S (*11*).

Cerenkov luminescence imaging (CLI) is based on the detection of photons produced in a dielectric medium, when the medium interacts with β-particles traveling at a speed greater than the velocity of light. Cerenkov luminescence comprises predominantly ultraviolet and blue light, which is highly susceptible to attenuation in biologic tissue, therefore limiting CLI to the detection of signals emitted in superficial tissue layers (*16,17*). In the context of RP, the detected signals can accordingly be indicative of a PRM (*13,14*).

The feasibility and safety of ^{68}Ga-PSMA CLI have recently been demonstrated in RP. However, so far, only feasibility studies have been described, and larger multicenter randomized trials are pending. In addition, clinical application without intraoperative tracer injection is challenged by the short half-life of ^{68}Ga and the time required for prostate removal (*18–20*). ^{18}F-PSMA CLI would easily overcome this restriction with respect to the half-life. However, 1 limitation for ^{18}F may arise from having a theoretically 26-fold lower Cherenkov light yield compared with ^{68}Ga, which is caused by the lower β^+-energy (*21*).

An alternative way of generating photons that can be detected by the same imaging system as in CLI may be introduced by adding a scintillator between the specimen and the detectors. In this novel approach, called flexible autoradiography (FAR), scintillations are produced by a micrometers-thick flexible scintillating film draped over an excised specimen (Supplemental Fig. 1; supplemental materials are available at http://jnm.snmjournals.org). The physical principle differs from CLI in that the high-energy β-particles from the radiotracer interact with the scintillator, which subsequently produces photons in the visible light spectrum. Since the Cerenkov photons are also detected, this is referred to as FAR CLI. The main advantage of a flexible scintillation film over conventional rigid autoradiography techniques is that the former conforms to the shape of the excised specimen. By maximizing the contact area, sectioning of the tissue can be eliminated and signal intensity increased. The thinness of a flexible scintillator makes it insensitive to the ^{18}F 511-keV γ-photons (*22,23*). FAR CLI in an in vitro preclinical application increased the signal for ^{18}F by a factor of 11, allowing for further development of ^{18}F tracers also in the context of intraoperative imaging (*24*). The behavior of ^{18}F-PSMA CLI and ^{18}F-PSMA-FAR CLI in human perfused tissue undergoing RP is unknown.

The primary objective of the study was to investigate the feasibility of both modalities in RP, with examination of the minimum detectable activity level as a secondary objective. We first investigated the applicability of both imaging modalities—^{18}F-PSMA CLI and ^{18}F-PSMA-FAR CLI—in a mouse model that possesses optical characteristics similar to those of prostate tissue, and we then translated the findings to RP. To our knowledge, we are the first to perform CLI and FAR CLI using ^{18}F-PSMA in PC patients.

MATERIALS AND METHODS

To investigate the imaging behavior and minimum detectable activity concentration (AC) of ^{18}F-PSMA-1007 in CLI and FAR CLI, a 2-step approach was used (Fig. 1). First, multimodal PET/CT (β-Cube/X-Cube; Molecubes), as well as CLI and FAR CLI imaging with the LightPath system (Lightpoint Medical Ltd.), was performed on mice bearing subcutaneous PSMA-avid RM1-PGLS tumors (*25*). Subsequently, the findings were transferred and evaluated in RP. The studies were formally approved by the North Rhine–Westphalia State Agency for Nature, Environment, and Consumer (LANUV; Z.81-02.04.2018.A090) and the local Ethical Committee of the University of Duisburg–Essen (19-8749-BO). Additionally, a dilution series with ^{18}F-PSMA was prepared and used to measure CLI and FAR CLI in Eppendorf tubes and assess the device's performance with respect to linearity and minimum detectable AC in the absence of tissue.

Preclinical Setup: Mouse Model

RM1-PGLS cells were cultured in Rosewell Park Memorial Institute 1640 medium/10% fetal bovine serum at 37°C and 5% CO_2. Contamination with *Mycoplasma* was excluded using the Venor GeM *Mycoplasma* detection kit (Sigma Aldrich).

Male C57BL/6 mice (5–12 wk old; Charles River) were bred and housed under pathogen-free conditions, with food and water ad libitum and a 12 h–12 h light–dark cycle. Eight days before intraperitoneal injection of 2.61 MBq (range, 2.02–3.06 MBq) of ^{18}F-PSMA-1007, RM1-PGLS (0.1×10^6 cells in 1:1 Matrigel [Corning]:phosphate-buffered saline) were injected subcutaneously into the shoulder region of 5 mice. Small-animal PET/CT was performed 2 h after injection, and reconstructed ACs were used to correlate the CLI and FAR CLI signals. Immediately after PET/CT, the mice were killed for CLI and FAR CLI. The first CLI/FAR CLI imaging set-up included the whole mouse to visualize both kidneys and the shoulder region in the LightPath system. The kidneys and tumor tissue were then excised and reexamined with the LightPath system. The main rationale

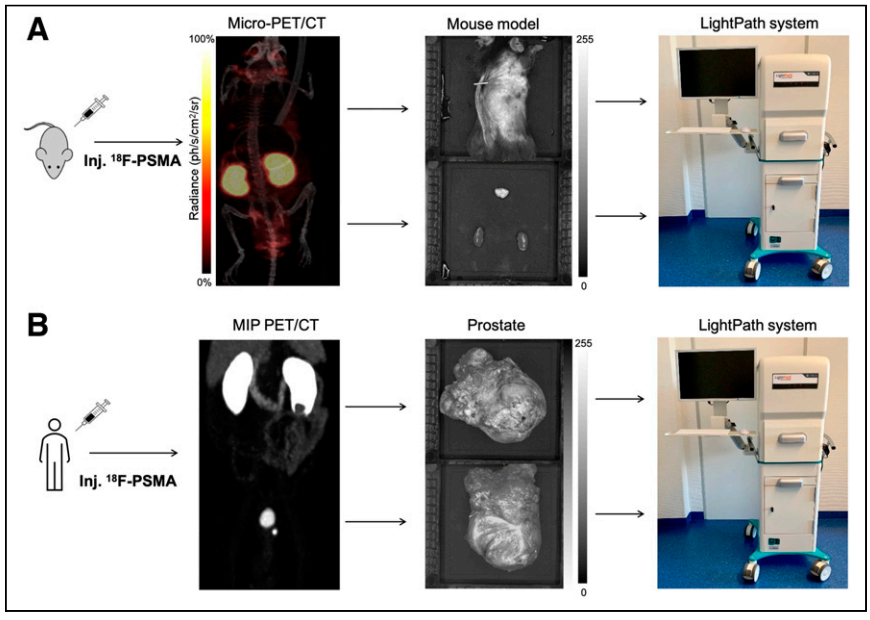

FIGURE 1. Study design. (A) Injection of ^{18}F-PSMA into tumor-bearing mice. Two hours afterward, small-animal PET/CT was performed. Next, CLI and FAR of whole mouse were acquired, followed by analysis of excised kidneys and PC tissue. (B) In second approach, prostate specimen in patients undergoing RP was examined, with direct preoperative ^{18}F-PSMA PET/CT. Removal of prostate was followed by immediate examination of intact prostate specimen and target lesion (after incision) by CLI and FAR. MIP = maximum-intensity projection.

for using mouse specimens was that, in principle, they should have optical characteristics similar to those of the prostate and therefore provide a more valid surrogate for sensitivity than Eppendorf tubes, for example (*26*).

Clinical Setup: RP

Patients with histologically confirmed PC without metastases on conventional staging were scheduled for RP. On the day of surgery, ^{18}F-PSMA-1007 was injected intravenously for routine PSMA PET staging before surgery (*27*). Approximately 60 min after injection, PET/CT was performed and assessed by dedicated specialists in nuclear medicine. In the case of high-volume metastatic disease on PET/CT, same-day surgery would have been cancelled. After PET/CT, RP was performed by 1 experienced surgeon ahead of extended pelvic lymph node dissection to minimize signal intensity reduction from radiotracer decay in the time between ^{18}F-PSMA injection and CLI/FAR CLI imaging. After retrieval of the prostate, it was rinsed twice to clear any potential radioactive contamination from blood or urine, followed by imaging of the entire specimen. Two or 3 images were necessary to capture all sides of the prostate. MRI-guided incision above the index lesion was then performed, followed by imaging (CLI and FAR CLI) of the lesion. This allowed direct examination of the tumor tissue with assessment of the present luminescence, corresponding to a PRM. On completion of the investigational imaging, the prostatectomy specimen was sent for postoperative histopathologic analysis. We recently demonstrated that a single injection of ^{68}Ga-PSMA as part of the PET/CT/CLI procedure is associated with acceptable occupational exposure (*28*). According to the model, the use of ^{18}F-PSMA would increase occupational exposure comparatively to ^{68}Ga-PSMA, allowing for 117 procedures before reaching the lower occupational yearly limit of 6 mSv. The exposed personnel are continuously monitored in accordance with the legal requirements. Because of the design of this feasibility study, the surgical course remained unaffected by the intraoperative imaging results, and no further tissue was resected if positive margins were suspected.

Imaging and Image Analysis

The LightPath system, an in vitro diagnostic device, was used to visualize the location of ^{18}F-PSMA for CLI and FAR CLI. This system was further described by Ciarrocchi et al. (*29*). Both a luminescence image and a gray-scaled image of the specimen were captured through the system. Both CLI and FAR CLI were acquired in a standardized manner, with an acquisition time of 300 s, 8 × 8 binning, and no optical filter (*29*). The images had to be acquired in a light-tight chamber. The 12-μm-thick flexible scintillating film (Lightpoint Medical Ltd.) used in FAR CLI consisted of a multilayer sandwich construction as follows: 3 μm of mylar, 6 μm of P43 scintillating phosphor, and 3 μm of mylar (*22*).

Background signals and elevated signals of both imaging modalities were subsequently analyzed using PMOD (version 3.204; PMOD Technologies LLC). Mean radiance (photons/s/cm^2/sr) was measured in regions of interest with a 50% threshold. Two-dimensional regions of interest were selected in areas showing increased signal intensity (tumor) or no increased signal (tissue background) to calculate contrast-to-noise ratios (CNRs):

$$\text{CNR} = \frac{\text{tumor average} - \text{background average}}{\text{background SD}}.$$

In the absence of increased signal, the corresponding MRI-informed target lesion was contoured. In terms of detectability, foci were considered sufficiently visible with a CNR of 5 or more, a condition also referred to as the Rose criterion (*30*).

Statistical Analysis

Numeric variables were summarized with median values and interquartile ranges, and categoric variables were summarized with proportions (%). To compare the medians of nonparametric data, the Mann–Whitney *U* test was used for 2 groups. The Spearman correlation coefficient was used for correlation, with significance set at a *P* value of less than 0.05. The CLI CNR values were plotted as a function of the measured PET mean AC (decay-corrected to the time of CLI), and a linear regression model (least-squares method) was applied, constraining the model to pass at the origin (i.e., the condition in which there is no tracer, when the CNR output should be close to zero). Statistical analysis was performed with SPSS Statistics, version 26 (IBM).

RESULTS

Preclinical Setup: Mouse Model

Our in vitro assay with ^{18}F-PSMA demonstrated activity levels in Eppendorf tubes of up to 5.46 kBq/mL for CLI and 1.60 kBq/mL for FAR CLI (Supplemental Fig. 2). Linear regression between AC and CNR revealed r^2 values of 0.91 and 0.85 (both $P < 0.0001$).

In small-animal PET/CT, the reconstructed median AC 2 h after tracer administration was 651.72, 608.56, and 52.99, for the left kidney, right kidney, and PC tissue, respectively. Linear regression between CLI CNR and the decay-corrected PET AC of the small-animal PET/CT images 2 h after injection demonstrated r^2 values of 0.92 ($P < 0.0001$) and 0.62 ($P < 0.0001$) for the excised organs and whole mouse, respectively (Fig. 2).

During examination of the whole mouse, visualization of the subcutaneous PC tissue was not possible on CLI in any of the 5 cases. In FAR CLI, 3 cases showed a weak signal with a minimum AC of 22.16 kBq/mL at a CNR of 7.07. Regarding the examination of excised PC tissue, on CLI no signal was detectable with a maximum AC of up to 15 kBq/mL. In contrast, ^{18}F-PSMA uptake could be visualized by FAR CLI in all 5 PC samples, with a lowest detected AC and CNR of 7.25 kBq/mL and 5.48, respectively (Fig. 3). Despite the different detection threshold, there was no statistical difference between FAR CLI and CLI ($P < 0.09$), and least-squares linear regression showed good agreement between the two modalities ($r^2 = 0.75$; $P = 0.05$). Direct examination of high ACs revealed a contiguous uptake region in the kidneys and PC tissue on FAR CLI. The signal from the PC tumors could be visualized reliably in the single examination (Supplemental Fig. 3). Consequently, the specimens were placed farther apart in the subsequent measurements.

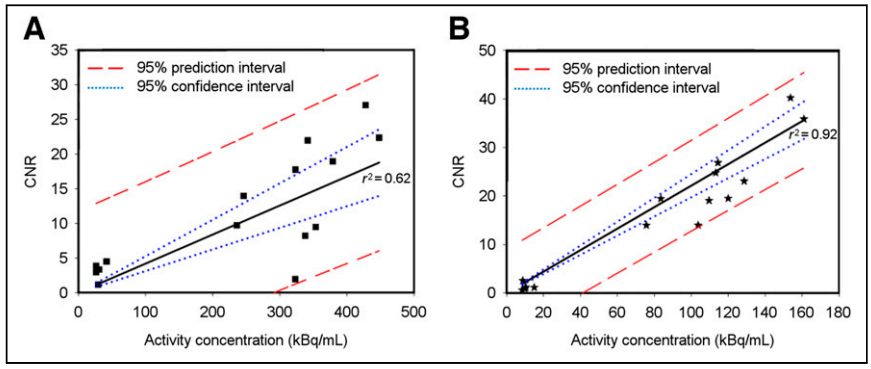

FIGURE 2. Linear regression of preclinical CLI with standardized imaging protocol. CNR is plotted against small-animal PET/CT AC. (A) PET vs. whole-mouse CLI comparison. (B) PET vs. excised kidneys and PC tissue comparison.

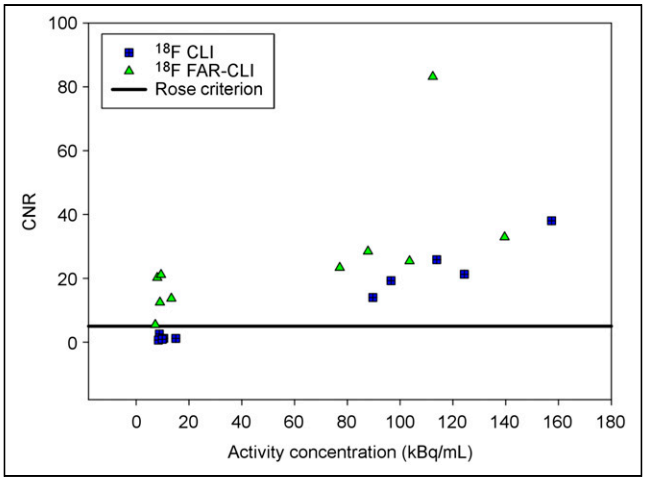

FIGURE 3. Visual detectability of excised kidneys and PC tissue. CNR is plotted against small-animal PET/CT AC. Highest AC region corresponds to signals from kidneys, whereas lowest cluster refers to PC signals. Foci with CNR ≥ 5 were considered detectable (Rose criterion).

At time of imaging, there was no significant difference in tracer AC between CLI and FAR CLI, but there was a significant increase in the CNR of visible foci (Supplemental Table 1). There was a strong correlation between a higher AC of the excised kidneys and PC tissue with a higher CNR, with a Spearman ρ of 0.783 ($P < 0.001$) for CLI and 0.712 ($P < 0.001$) for FAR CLI. Examination of the whole mouse also showed a strong correlation, with a Spearman ρ of 0.559 ($P < 0.001$) for CLI and 0.379 ($P = 0.01$) for FAR CLI.

Clinical Setup: RP

Seven patients were included in this feasibility study, among whom 6 had a high risk of progression according to the guidelines of the National Comprehensive Cancer Network (*31*). Imaging and patient characteristics are displayed in Table 1.

CLI detected a median of 2 lesions on the prostate surface, 1 of which was always at the bladder neck, with a median CNR of 33.96 (Table 2). In terms of CNR and number of lesions detected, there was a significant reduction using FAR CLI ($P = 0.02$) at comparable AC levels. Two patients showed PRMs after histopathologic evaluation. The PRMs consisted once of an International Society of Urological Pathology Gleason Grading Group (ISUP-GGG) of 4 with a diameter of 2 mm. Both CLI and FAR CLI showed no signal in the corresponding location. The second PRM, with an ISUP-GGG of 1 and a diameter of 1 mm, also showed no corresponding image morphologic correlate on CLI and FAR CLI. The PRM was histopathologically located at the right dorsal apex. CLI and FAR CLI showed a suggestive signal at the right lateral apex (Supplemental Fig. 4).

After incision over the MRI-informed index lesion, no luminescence on CLI was detectable, with a median CNR of 0.26. The mean gain in the sensitivity of FAR CLI in comparison to CLI was evaluated for Eppendorf tubes by calculating the fold increase in radiance normalized for AC. FAR CLI showed an approximately 2.1-fold radiance enhancement (Supplemental Fig. 5). Median AC at the time of incision was 3.06 kBq/mL. In contrast, a suggestive luminescence of PC was detectable in 6 of 7 patients on FAR CLI (Fig. 4). The AC of the 1 missed index lesion was 1.85 kBq/mL, resulting in a detection limit of at least 2.06 kBq/mL with a median CNR of 8.78. Direct anatomic correlation was challenging because of the scintillator overlay.

TABLE 1
Nuclear Medicine and Patient Characteristics

Characteristic	Data
Imaging	
Activity injected (MBq)	312 (280–332)
Tracer activity at PET/CT (kBq/mL)	17.71 (12.46–34)
Activity at CLI (kBq/mL)	3.54 (2.57–6.91)
Time from injection to CLI/FAR CLI (min)	329 (308–333)
CNR	
CLI	0.26 (0–1.5)
FAR CLI	9.13 (4.13–19.23)
Patient	
Age (y)	65.14 (63–67)
Initial PSA (ng/mL)	11 (5.1–22)
NCCN risk at biopsy	
High risk	6 (86%)
Intermediate risk	1 (14%)
NCCN risk score at final histopathology	
High risk	5 (71%)
Intermediate risk	2 (29%)
Resection status	
R1 resection	2 (29%)
R0 resection	5 (71%)

PSA = prostate-specific antigen; NCCN = National Comprehensive Cancer Network.

Qualitative data are number and percentage; continuous data are median and interquartile range.

DISCUSSION

In mice with subcutaneous PSMA-avid PC, different levels of AC were evaluated in terms of visualization. Because of the difference in tracer uptake between kidneys and PC tissue, it was possible to generate a broad spectrum of signals over time. Previously, Olde Heuvel et al. described a detection limit of 3.42 kBq/mL for ^{18}F-CLI in vitro (*32*). Our in vitro assay demonstrated similar findings, with a detection limit in Eppendorf tubes of 5.46 kBq/mL for CLI and 1.60 kBq/mL for FAR CLI. Such a radiance enhancement was also reported by Pratt et al., who evaluated nanoparticles in the presence of β-emitters (*33*). In contrast, no significant CLI signal from PC tissue up to 15 kBq/mL was observed in our mouse model. The discrepancies between in vitro and mouse measurements can be explained by the absorption (e.g., by hemoglobin) and scattering in biologic tissues, severely limiting sensitivity (*34*). On the basis of our study design with preoperative tracer injection and an estimated time from injection to prostate examination of approximately 5 h, ACs above 15 kBq/mL are not expected. In contrast to CLI, FAR CLI visualized PC tissue up to an activity of 7.25 kBq/mL. A clear

TABLE 2
Cerenkov Luminescence and Autoradiography Imaging Measurements of Prostatectomy Specimen with Corresponding Activity Levels

Parameter	CLI	FAR CLI	*P*
Intact specimen (n = 7)			
Activity (kBq/mL)	3.53 (2.57–6.91)	3.95 (2.16–7.22)	NS
CNR	33.96 (15.71–43.29)	6.13 (4.07–21.43)	0.02
Lesions	2 (1–2)	1 (0.5–1)	0.02
Incised specimen (n = 7)			
Activity (kBq/mL)	3.06 (1.98–5.98)	2.8 (2.06–5.72)	NS
CNR	0.26 (0–1.5)	9.53 (4.13–19.23)	0.002

CNR = contrast-to-noise-ratio; NS = not significant.
Data are median and interquartile range. Significance is set at $P < 0.05$.

discrimination was possible, with a median CNR of 5.48, so that FAR CLI seems to be a promising modality for low AC levels. We were able to show that subcutaneous (at <1 mm depth) PC tumors could be visualized down to the lowest measured AC of 23.02 kBq/mL on FAR CLI.

Next, we tested FAR CLI in men undergoing RP. This first-in-men study investigated the feasibility of assessing tumor margin status and of evaluating minimum detection limits.

After incision, no increased signal on CLI was visible. CLI using an ^{18}F-PSMA did not provide any useful signals, only luminescence artifacts. In contrast, with the aid of the flexible scintillator, FAR CLI detected cancer foci. The minimum detectable AC was 2.06 kBq/mL, with a CNR of 10.84. On this basis, good detection of PRMs should be assumed. However, the use of FAR CLI for PRM assessment is challenging. PRMs were found in 2 patients. In 1 patient, histology demonstrated a 2-mm positive margin with an ISUP-GGG of 4 at the left seminal vesicle plateau, but even with FAR CLI, no signal was visible in this area. The second PRM, with an ISUP-GGG of 1 and a length of 1 mm, also showed no corresponding correlate on FAR CLI.

Jurrius et al. also investigated the use of FAR to assess resection margins (*23*). In the context of breast-conserving surgery with ^{18}F-FDG, an overall accuracy of 80.5% was shown, with a sensitivity of 46.2%. Although a direct comparison between breast cancer and PC is difficult, our results do not show the same benefit for FAR CLI. On the one hand, this may be due to tumor biology; on the other hand, it may be related to the study design. A major difference is the timing between tracer injection and measurement of CLI or FAR CLI activity. In our study, measurements were taken about 2 h later than in the work of Jurrius et al.

In principle, every radioguided-surgery technique requires a high CNR, high sensitivity, and user friendliness to provide a net benefit for patients and surgeons in routine care. CLI provides good surface contrast but, as has been shown in this report, insufficient sensitivity at very low activities, mainly because of tissue light absorption. Although FAR CLI, is able to compensate for the

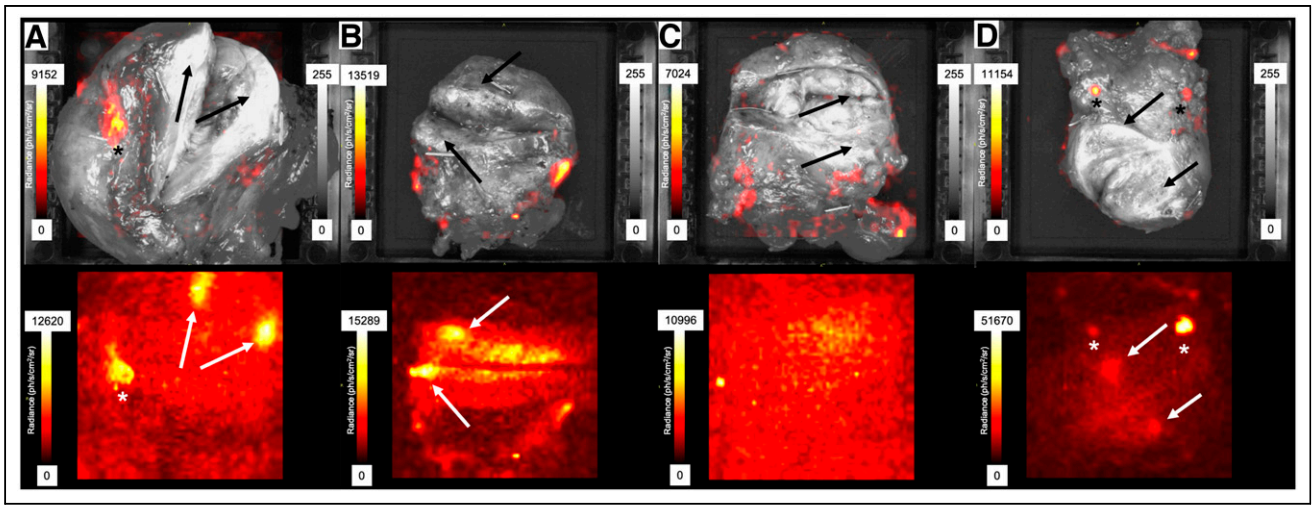

FIGURE 4. Images of incised prostate specimens: CLI with overlying gray-scale photographs (top) and FAR CLI (bottom). CLI shows no hot spots (arrows) in PC lesions seen on FAR CLI (arrows). Artificial signals in CLI and correlating FAR CLI signals are indicated (*). Histopathology proved absence of PC at surface. FAR CLI in A and B shows good signal, with CNRs of 9.13 and 23.03. FAR CLI in C shows no increased signal detectable in PC, with activity of 1.85 kBq/mL and corresponding CNR of 3.69. FAR CLI in D shows increased signal, with CNR of 10.84 at activity of 2.06 kBq/mL.

lack of sensitivity by increasing the net light output per emitted β-particle, the result is imaged foci that have a lower spatial resolution, making it difficult to discriminate closely adjacent regions of uptake. Furthermore, because CLI and FAR CLI are highly sensitive to ambient light, measurements can be made only in a light-tight chamber. This limitation must be considered when designing further implementations of the system. A possible improvement to the presented method might be achieved by topical application of nanoparticles. Pratt et al. described the advantages of Gd_2O_3 and Eu_2O_3, which showed the greatest enhancement in radiance. The combination of Gd_2O_3 and Eu_2O_3 with ^{68}Ga and ^{18}F, respectively, produced distinct visible emission peaks (*33*).

Additional limitations of our work deserve further discussion. In our study setting, ^{18}F-PSMA represents a suboptimal tracer because of very low activity in the context of RP. Although, in contrast to other tracers, the half-life is prolonged, the emitted energy is lower. Adjustment of the current workflow is necessary to achieve higher activity levels at the time of RP through optimization of dosing and timing. However, radiation exposure of medical personnel and patients must be considered, as well as possible negative effects on specificity. The fact that, in most of the patients, a signal was detected on FAR CLI after incision demonstrated the feasibility of ^{18}F-PSMA-FAR CLI. When there are suggestive findings, CLI might subsequently be used for surface assessment. The extent to which this can be applied clinically remains to be investigated. The flexible scintillation film is semiopaque and thus obscures the white-light reference image of the sample, presenting a challenge for accurate correlation of the FAR CLI signal with the exact anatomic location on the sample.

CONCLUSION

Detection of PC using ^{18}F-PSMA-FAR CLI is possible—even at low activity levels down to 2.06 kBq/mL. However, anatomic correlation is difficult and detection of PRMs failed. ^{18}F-PSMA CLI had no value in this setup.

DISCLOSURE

Claudia Kesch reports consulting fees from Apogepha and research funding from Advanced Accelerator Applications (Novartis). Stephan Tschirdewahn reports personal and travel fees from Ipsen, Eisai, Bayer, Janssen, Novartis, Bristol-Myers-Squibb, and BrachySolutions and research funding from Ipsen. Jan Radtke reports personal and travel fees from Invivo Uronav, Bender Group, Beckelmann and Partners, and Saegeling Medizintechnik and research funding from Advanced Accelerator Applications and Novartis. Ken Herrmann reports personal fees from Bayer, Sofie Biosciences, SIRTEX, Adacap, Curium, Endocyte and BTG. Wolfgang Fendler reports fees from SOFIE Bioscience (research funding), Janssen (consultant, speakers' bureau), Calyx (consultant), Bayer (consultant, speakers' bureau, research funding), and Parexel (image review) outside the submitted work. Boris Hadaschik reports personal fees from ABX, Bayer, LightPoint Medical Inc., Janssen R&D, Bristol-Myers-Squibb, and Astellas; research funding from Profound Medical, German Cancer Aid, German Research Foundation, Janssen R&D, Bristol-Myers-Squibb, MSD, Pfizer, and Astellas; and travel fees from AstraZeneca, Janssen R&D, and Astellas. This work was supported by the Deutsche Forschungsgemeinschaft (project HA 5160/5-1). No other potential conflict of interest relevant to this article was reported.

KEY POINTS

QUESTION: Are CLI and FAR CLI useful for displaying PC cells close to or at the surface of prostatectomy specimens?

PERTINENT FINDINGS: In this feasibility study, 7 patients undergoing RP and an ^{18}F-PSMA PET/CT scan on the same day were analyzed for suggestive intensity levels. FAR CLI, in contrast to CLI, was able to clearly highlight PC cells from surrounding tissue after incision. However, detection of PC in PRMs was not possible by either modality.

IMPLICATIONS FOR PATIENT CARE: ^{18}F-CLI has no value for the detection of resection margins in a preoperative ^{18}F-PSMA administration protocol. ^{18}F-FAR CLI is possible, but without meaningful clinical benefit.

REFERENCES

1. Prostate cancer. European Association of Urology website. https://uroweb.org/guidelines/prostate-cancer. Published 2022. Accessed December 22, 2022.
2. Iczkowski KA, Lucia MS. Frequency of positive surgical margin at prostatectomy and its effect on patient outcome. *Prostate Cancer.* 2011;2011:673021.
3. Yossepowitch O, Briganti A, Eastham JA, et al. Positive surgical margins after radical prostatectomy: a systematic review and contemporary update. *Eur Urol.* 2014; 65:303–313.
4. Schlomm T, Tennstedt P, Huxhold C, et al. Neurovascular structure-adjacent frozen-section examination (NeuroSAFE) increases nerve-sparing frequency and reduces positive surgical margins in open and robot-assisted laparoscopic radical prostatectomy: experience after 11,069 consecutive patients. *Eur Urol.* 2012;62:333–340.
5. Nyarangi-Dix J, Wiesenfarth M, Bonekamp D, et al. Combined clinical parameters and multiparametric magnetic resonance imaging for the prediction of extraprostatic disease: a risk model for patient-tailored risk stratification when planning radical prostatectomy. *Eur Urol Focus.* 2020;6:1205–1212.
6. Petralia G, Musi G, Padhani AR, et al. Robot-assisted radical prostatectomy: multiparametric MR imaging-directed intraoperative frozen-section analysis to reduce the rate of positive surgical margins. *Radiology.* 2015;274:434–444.
7. Collamati F, van Oosterom MN, Hadaschik BA, Fragoso Costa P, Darr C. Beta radioguided surgery: towards routine implementation? *Q J Nucl Med Mol Imaging.* 2021;65:229–243.
8. Olde Heuvel J, de Wit-van der Veen BJ, Huizing DMV, et al. State-of-the-art intraoperative imaging technologies for prostate margin assessment: a systematic review. *Eur Urol Focus.* 2021;7:733–741.
9. Meershoek P, van Oosterom MN, Simon H, et al. Robot-assisted laparoscopic surgery using DROP-IN radioguidance: first-in-human translation. *Eur J Nucl Med Mol Imaging.* 2019;46:49–53.
10. Maurer T, Robu S, Schottelius M, et al. ^{99m}technetium-based prostate-specific membrane antigen-radioguided surgery in recurrent prostate cancer. *Eur Urol.* 2019;75:659–666.
11. Maurer T, Graefen M, van der Poel H, et al. Prostate-specific membrane antigen-guided surgery. *J Nucl Med.* 2020;61:6–12.
12. Knipper S, Mehdi Irai M, Simon R, et al. Cohort study of oligorecurrent prostate cancer patients: oncological outcomes of patients treated with salvage lymph node dissection via prostate-specific membrane antigen-radioguided surgery. *Eur Urol.* 2023;83:62–69.
13. Koehler D, Sauer M, Klutmann S, et al. Feasibility of ^{99m}Tc-MIP-1404 for SPECT/CT imaging and subsequent PSMA-radioguided surgery in early biochemical recurrent prostate cancer: a case series of 9 patients. *J Nucl Med.* July 14, 2022 [Epub ahead of print].
14. Collamati F, van Oosterom MN, De Simoni M, et al. A DROP-IN beta probe for robot-assisted ^{68}Ga-PSMA radioguided surgery: first ex vivo technology evaluation using prostate cancer specimens. *EJNMMI Res.* 2020;10:92
15. Debacker JM, Schelfhout V, Brochez L, et al. High-resolution ^{18}F-FDG PET/CT for assessing three-dimensional intraoperative margins status in malignancies of the head and neck, a proof-of-concept. *J Clin Med.* 2021;10:3737.
16. Grootendorst MR, Cariati M, Pinder SE, et al. Intraoperative assessment of tumor resection margins in breast-conserving surgery using ^{18}F-FDG Cerenkov luminescence imaging: a first-in-human feasibility study. *J Nucl Med.* 2017;58:891–898.
17. Chin PT, Welling MM, Meskers SC, Valdes Olmos RA, Tanke H, van Leeuwen FW. Optical imaging as an expansion of nuclear medicine: Cerenkov-based luminescence vs fluorescence-based luminescence. *Eur J Nucl Med Mol Imaging.* 2013;40:1283–1291.

18. Darr C, Harke NN, Radtke JP, et al. Intraoperative ^{68}Ga-PSMA Cerenkov luminescence imaging for surgical margins in radical prostatectomy: a feasibility study. *J Nucl Med.* 2020;61:1500–1506.
19. Olde Heuvel J, de Wit-van der Veen BJ, van der Poel HG, et al. ^{68}Ga-PSMA Cerenkov luminescence imaging in primary prostate cancer: first-in-man series. *Eur J Nucl Med Mol Imaging.* 2020;47:2624–2632.
20. Darr C, Fragoso Costa P, Kesch C, et al. Prostate specific membrane antigen (PSMA)-radio guided surgery using Cerenkov luminescence imaging: utilization of a short-pass filter to reduce technical pitfalls. *Transl Androl Urol.* 2021;10: 3972–3985.
21. Gill RK, Mitchell GS, Cherry SR. Computed Cerenkov luminescence yields for radionuclides used in biology and medicine. *Phys Med Biol.* 2015;60:4263–4280.
22. Vyas KN, Grootendorst M, Mertzanidou T, et al. Flexible scintillator autoradiography for tumor margin inspection using ^{18}F-FDG. In: *Proceedings Volume 10478, Molecular-Guided Surgery: Molecules, Devices, and Applications IV.* SPIE; 2018:1–12.
23. Jurrius P, Grootendorst MR, Krotewicz M, et al. Intraoperative [^{18}F]FDG flexible autoradiography for tumour margin assessment in breast-conserving surgery: a first-in-human multicentre feasibility study. *EJNMMI Res.* 2021;11:28.
24. Annual Congress of the European Association of Nuclear Medicine. October 13–17, 2018, Düsseldorf, Germany. *Eur J Nucl Med Mol Imaging.* 2018;45:1–844.
25. Lückerath K, Stuparu AD, Wei L, et al. Detection threshold and reproducibility of ^{68}Ga-PSMA11 PET/CT in a mouse model of prostate cancer. *J Nucl Med.* 2018; 59:1392–1397.
26. olde Heuvel J, de Wit-van der Veen L, Tuch D, Vyas K, Stokkel M, Slump C. Performance evaluation of Cerenkov luminescence imaging: a comparison of ^{68}Ga with ^{18}F [abstract]. *J Nucl Med.* 2018;59(suppl 1):365.
27. Fendler WP, Eiber M, Beheshti M, et al. ^{68}Ga-PSMA PET/CT: joint EANM and SNMMI procedure guideline for prostate cancer imaging: version 1.0. *Eur J Nucl Med Mol Imaging.* 2017;44:1014–1024.
28. Costa PF, Fendler WP, Herrmann K, et al. Radiation protection and occupational exposure on ^{68}Ga-PSMA-11-based Cerenkov luminescence imaging procedures in robot-assisted prostatectomy. *J Nucl Med.* 2022;63:1349–1356.
29. Ciarrocchi E, Vanhove C, Descamps B, De Lombaerde S, Vandenberghe S, Belcari N. Performance evaluation of the LightPath imaging system for intra-operative Cerenkov luminescence imaging. *Phys Med.* 2018;52:122–128.
30. Bright DS, Newbury DE, Steel EB. Visibility of objects in computer simulations of noisy micrographs. *J Microsc.* 1998;189:25–42.
31. Prostate cancer (version 1.2023). National Comprehensive Cancer Network website. https://www.nccn.org/professionals/physician_gls/pdf/prostate.pdf. Published September 16, 2022. Accessed December 22, 2022.
32. Olde Heuvel J, de Wit-van der Veen BJ, Vyas KN, et al. Performance evaluation of Cerenkov luminescence imaging: a comparison of ^{68}Ga with ^{18}F. *EJNMMI Phys.* 2019;6:17.
33. Pratt EC, Shaffer TM, Zhang Q, Drain CM, Grimm J. Nanoparticles as multimodal photon transducers of ionizing radiation. *Nat Nanotechnol.* 2018;13:418–426.
34. Ciarrocchi E, Belcari N. Cerenkov luminescence imaging: physics principles and potential applications in biomedical sciences. *EJNMMI Phys.* 2017;4:14.